This manuscript was published as:
Kim S-G+, Chung MK, Seo SH, Schaefer SM, van Reekum CM, Davidson RJ. (2011, Nov). Heat kernel smoothing via Laplace-Beltrami eigenfunctions and its application to subcortical structure modeling. In Ho YS (Ed.): Pacific-Rim Symposium on Image and Video Technology (PSIVT), Part 1, Lecture Notes in Computer Science (LNCS), 7087: pp. 36-57, Springer, Heidelberg. (acceptance rate: 42%; selected for +oral presentation) doi: 10.1007/978-3-642-25367-6_4

Heat Kernel Smoothing via Laplace-Beltrami Eigenfunctions and Its Application to Subcortical Structure Modeling

Seung-Goo Kim[a], Moo K. Chung[a,b,c] ,
Stacey M. Schaefer[c], and Richard J. Davidson[c,d]

[a]Department of Brain and Cognitive Sciences
Seoul National University, Korea

[b]Department of Biostatistics and Medical Informatics
[c]Waisman Laboratory for Brain Imaging and Behavior
[d]Department of Psychology and Psychiatry
University of Wisconsin, Madison, WI, USA.

Abstract. We present a new subcortical structure shape modeling framework using heat kernel smoothing constructed with the Laplace-Beltrami eigenfunctions. The proposed framework is applied in investigating the influence of age and gender on amygdala and hippocampus shape in the middle age and elderly population. We detected the significant age effect on hippocampus in accordance with the previous studies. In addition, we also detected the significant gender effect on amygdala. Since we did not find any differences in the traditional volumetric methods, it demonstrates the benefit of the current framework over the traditional methods.

1 Introduction

Amygdala and hippocampus are primary subcortical structures involved in regulating emotion and memory [1,2]. Age and gender could be major factors that affect the functions and structures of these regions, as implied by post-mortem studies [3]. Although the atrophy of brain tissues associated with the increase of age is reported in several hundreds subjects [4,5], the studies on the atrophy of amygdala and hippocampus are somewhat inconsistent. The volume reduction of amygdala and hippocampus due to aging has been found in some studies [6,7,8], while other studies did not find such association [9,4,10]. For the effect of gender, one reported significant differences in amygdala and hippocampus volume between the groups [11] whereas others failed to reproduce it [12]. The inconsistency in the traditional volumetric results may have been due to the different image processing and analysis pipelines used in these studies.

In most of those volumetric studies, the total volume of the amygdala or hippocampus was estimated by tracing the region of interest (ROI) manually and counting the number of voxels within the ROI. The limitation of the traditional

ROI-based volumetry is that it cannot determine if the volume difference is diffuse over the whole ROI or localized within specific regions of the ROI [13].

Although there are many computational methods to localize cortical shape characterization such as voxel-based morphometry (VBM) that compares gray matter or white matter density in a voxel-wise fashion across spatially normalized MRI volumes [14,15] and tensor-based morphometry (TBM) that uses the deformation field which is derived from the spatial normalization [13,16], there are not many literature on the local shape analysis of subcortical structures other than some studies [17,18,19] mostly due to the difficulty of segmentation of the subcortical structures.

Here we present a framework for subcortical structure shape analysis using heat kernel smoothing via Laplace-Beltrami eigenfunction while employing the deformation field that is derived from spatial normalization. Using the proposed framework, we examine the effect of age and gender on amygdala and hippocampus, contrasting the traditional volumetric analysis.

2 Method

We analyze the shape of subcortical structures as following steps: (1) obtain a population mean volume averaging the spatially normalized binary masks, and extract a template surface from the averaged binary volume (section 2.1), (2) interpolate the 3D displacement vector field onto the vertices of the surface meshes (section 2.2), (3) smooth out the length of displacement along the template surface using heat kernel smoothing to reduce noise, and smooth out the template surface as well for better visualization (section 2.2 and 2.2), (4) perform a general linear model testing the effect of age and gender. The details in each stage are discussed as below except the inference which is given in section 3.

2.1 Images and preprocessing

We have T1-weighted magnetic resonance images (MRI) of 69 middle age and elderly adults. The mean age is 58.04 $\pm$ 11.34 years, ranging between 38 to 79 years. The subjects are 23 males and 46 females. The amygdalae and hippocampi were manually segmented by an each individual rater.

We computed deformation field to normalize whole brain as well as regional masks. Brain tissues in the MRI scans were first segmented using Brain Extraction Tool (BET) [20]. Then the study specific template was constructed using the diffeomorphic shape and intensity averaging technique through Advanced Normalization Tools (ANTS) with cross-correlation as the similarity metric [21].

We normalized the masks into the template space applying the resulting deformation field. The normalized masks were then averaged building probabilistic maps and thresholded at 50%. Iso-surfaces were extracted using the *marching cube* algorithm [22] as implemented in MATLAB. The averaged masks and corresponding surfaces are shown in Fig. 1.

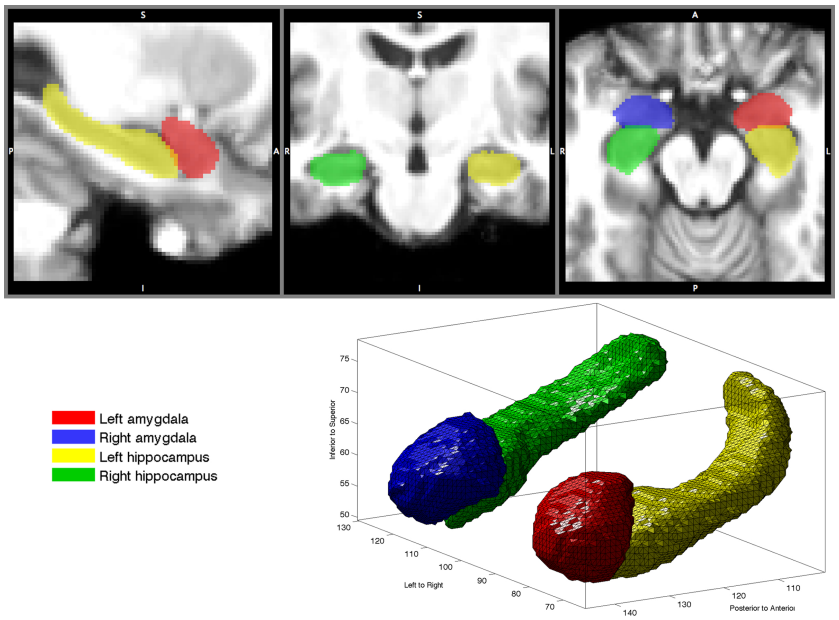

Fig. 1. Averaged masks overlaid on the template brain (upper row) and corresponding iso-surfaces (lower row).

2.2 Inverse deformation field interpolation

We have already computed inverse deformation field over whole brain that registers template image to an individual image during the spatial normalization. Thus we can obtain the inverse deformation field on each vertex by its smoothed coordinates using linear interpolation.

The inverse deformation fields on the vertices can deform the template surface to match the an individual surface, or the original manual segmentation, more or less. In this sense, we quantify how long the vertex on the template surface should be moved to match the individual surface with the L2-norm of the displacement vector field. WE USE THE LENGTH AS MEASURE FOR THOSE REASONS.... Other morphological measures are also available. In Chung et al.[16], surface-based morphological measures such as local area dilatation and local curvature dilatation by deformation have been used to measure the rate of expansion or reduction of cortical surface growth. AND... This corresponds to the local feature that describes structural shapes (Fig. 2).

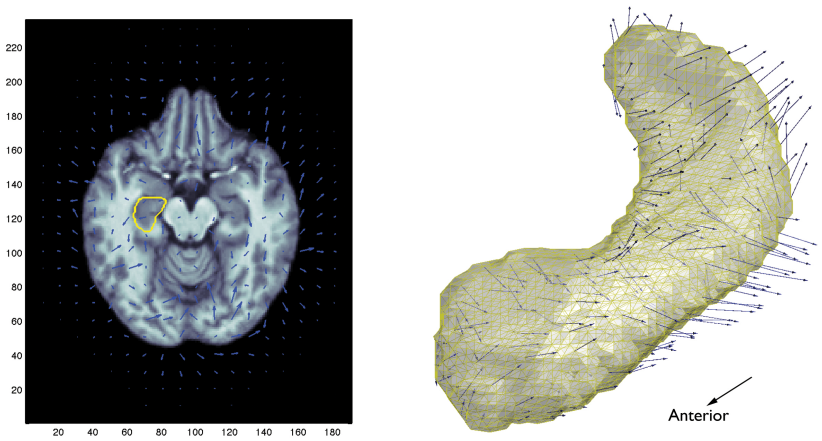

Fig. 2. Inverse deformation field (blue arrows) on an axial slice of the template brain (left) and its interpolation on the left hippocampus surface (right). Yellow contour in the left panel indicates the boundary of the averaged mask of the left hippocampus.

2.3 Heat kernel smoothing

The measurements on the extracted surface are noisy. So it is necessary to smooth out the measurements to increase the signal-to-noise ratio [13,16]. We employ heat kernel smoothing using Laplace-Beltrami eigenfunctions here

[23,24]. This method is anlaytic in a sense that heat kernel smoothing is formulated as a series expansion explicitly [24]. Thus we can avoid the instability associated with solving the diffusion equations numerically [25].

Consider a real-valued measure Y defined on a manifold $\mathcal{M} \subset \mathbb{R}^3$. We assume the following additive model on Y at a point p:

$$Y(p) = \theta(p) + \epsilon(p), \tag{1}$$

where $\theta(p)$ is the unknown mean signal and $\epsilon(p)$ is a zero-mean Gaussian random field. We may assume further $Y \in L^2(\mathcal{M})$, the space of square integrable functions on $\mathcal{M}$ with the inner product $\langle f, g \rangle = \int_{\mathcal{M}} f(p)g(p)d\mu(p)$, where μ is the Lebesgue measure such that $\mu(\mathcal{M})$ is the volume of $\mathcal{M}$. Solving

$$\Delta\psi_j = -\lambda_j\psi_j, \tag{2}$$

for the Laplace-Beltrami operator Δ on $\mathcal{M}$, we order eigenvalues $0 = \lambda_0 < \lambda_1 \geq \lambda_2 \cdots$ and corresponding eigenfunctions $\psi_0, \psi_1, \psi_2, \cdots$. Then the eigenfunctions ψ_j form an orthonormal basis in $L^2(\mathcal{M})$ [25].

Using the eigenfunctions, *heat kernel* $K_\sigma(p, q)$ is analytically given as

$$K_\sigma(p, q) = \sum_{j=0}^{\infty} e^{-\lambda\sigma}\psi_j(p)\psi_j(q), \tag{3}$$

where σ is the bandwidth of the kernel [26]. Then *heat kernel smoothing* of Y is given analytically as

$$K_\sigma * Y(p) = \sum_{j=0}^{\infty} e^{-\lambda\sigma}\beta_j\psi_j(p), \tag{4}$$

where $\beta_j = \langle Y, \psi_j(p) \rangle$ are Fourier coefficients. This is taken as the estimate for θ. Since the expansion (4) is a unique solution to isotropic heat diffusion [26], we can avoid the need to solve the diffusion using less stable numerical schemes such as the finite difference method [27].

2.4 Numerical Implementation

Generalized eigenvalue problem As the closed form expression for the eigenfunctions of the Laplace-Beltrami operator on an arbitrary curved surface is unknown, the eigenfunctions are numerically calculated by discretizing the LB operator. To solve the eigensystem (2), we need to discretize it on a triangular mesh using the Cotan formulation. Using the Cotan formulation, (2) is simplified as generalized eigenvalue problem:

$$\mathbf{C}\psi = \lambda\mathbf{A}\psi \tag{5}$$

where $\mathbf{C}$ is the stiffness matrix, $\mathbf{A}$ is the mass matrix and ψ is the unknown eigenfunction evaluated at mesh vertices. A few of first eigenfunctions for each surface are shown in Fig. 3.

Finite eigenfunction expansion Let $\mathcal{H}_k$ be the subspace spanned by up to k-th degree basis. Then an arbitrary measurement Y is estimated in the subspace $\mathcal{H}_k$ by minimizing the sum of squared residual:

$$\arg\min_{g\in\mathcal{H}_k} ||g - Y(p)||^2 = \sum_{j=0}^{k} \beta_j \psi_j(p). \tag{6}$$

Consider the triangular mesh for $\mathcal{M}$ with N_v nodes and let $\beta = (\beta_0, \cdots, \beta_k)'$ and $\mathbf{Y} = (Y(p_1), \cdots, Y(p_{N_v}))'$, for $k \leq N_v$. Then, we can represent (6) as the normal equation,

$$\mathbf{Y} = \beta\mathbf{\Psi}, \tag{7}$$

where $\mathbf{\Psi} = (\mathbf{\Psi}_0, \cdots, \mathbf{\Psi}_k)$ and $\mathbf{\Psi} = (\psi_j(p_1), \cdots, \psi_j(p_{N_v}))'$, and β is estimated in the least squares fashion, $\widehat{\beta} = (\mathbf{\Psi'\Psi})^{-1}\mathbf{\Psi'Y}$. Since the size of matrix $\mathbf{\Psi'\Psi}$ can become large when a large number of basis are necessary to obtain, it may be difficult to directly invert the matrix. So we have adopted a more general iterative strategy to overcome possible computational bottleneck for large k.

Iterative residual fitting algorithm Fourier coefficients are estimated using *iterative residual fitting* algorithm that utilizes the orthonormality of the eigenfunctions [28]. Decompose the subspace $\mathcal{H}_k$ into smaller subspaces as the direct sum $\mathcal{H}_k = \mathcal{I}_0 \oplus \cdots \mathcal{I}_k$, where each subspace $\mathcal{I}_j$ is the projection of $\mathcal{H}_k$ along the j-th eigenfunction. Instead of directly solving the normal equation (7), we project the normal equations into a smaller subspace $\mathcal{I}_j$ and find the corresponding β_j in an iterative fashion increasing the degree from 0 to k.

At degree k=0, we write $\mathbf{Y} = \mathbf{\Psi}_o\beta_0 + \mathbf{r}_0$, where $\mathbf{r}_0$ is the residual of estimating $\mathbf{Y}$ in subspace $\mathcal{I}_0$. Then, we estimate β_0 by minimizing the residual in the least squares fashion:

$$\widehat{\beta}_0 = (\mathbf{\Psi_0'\Psi_0})^{-1}\mathbf{\Psi_0'Y}. \tag{8}$$

At degree j, we have

$$\mathbf{r}_{j-1} = \mathbf{\Psi}_j\beta_j + \mathbf{r}_j, \tag{9}$$

where the previous residual $\mathbf{r}_{j-1} = \mathbf{Y} - \mathbf{\Psi}_0\widehat{\beta}_0 \cdots - \mathbf{\Psi}_{j-1}\widehat{\beta}_{j-1}$. The next residual $\mathbf{r}_j$ is then estimated as $\widehat{\beta}_j = (\mathbf{\Psi_j'\Psi_j})^{-1}\mathbf{\Psi_j'r_{j-1}}$.

In this paper, we choose the bandwidth of smoothing σ=0.5 and computed the finite eigenfunction expansion using up to 1000-th degree basis (Fig. 3). We smoothed the length of displacement vector field and the coordinates of template surfaces as well.

3 Results: General Linear Models on Surface Shapes

3.1 Traditional volumetric analysis

Given that the image resolution is 1 x 1 x 1 mm, the volume of amygdala and hippocampus were simply estimated by the number of voxels within the mask. In

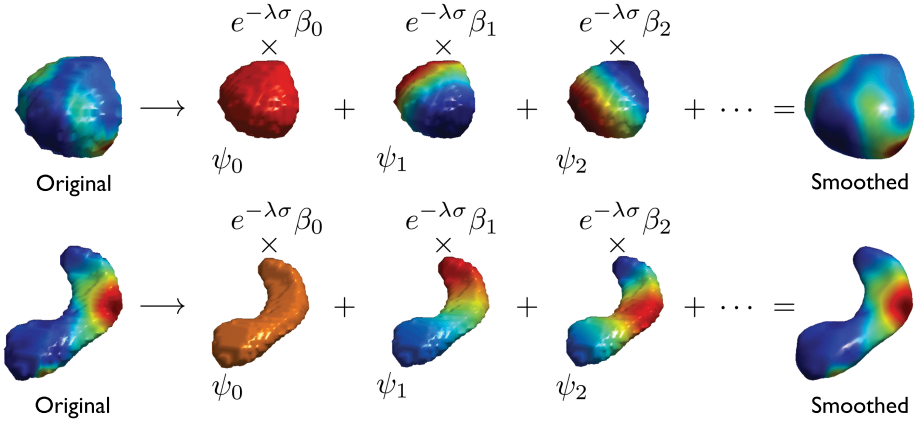

Fig. 3. Illustration for heat kernel smoothing using Laplace-Beltrami eigenfunctions. The left-most surfaces are original surfaces with the length of displacement vector field color-coded. First three eigenfunctions ψ_j are shown in the middle. The right-most surfaces are smoothed with $\sigma = 0.5$ with the smoothed length of displacement vector field.

order to account for the effect of variability in brain size, the brain volume was estimated excluding cerebellum. The brain volume significantly correlated with the amygdala volume(Left: r= 0.55, $p < 10^{-5}$; Right: r=0.49, $p < 10^{-4}$) and the hippocampus volume (Left: r= 0.59, $p < 10^{-7}$; Right: r=0.63, $p < 10^{-8}$).

We model the volume of regional structure y as

$$y = \beta_1 + \beta_2 \cdot \text{Brain} + \beta_3 \cdot \text{Age} + \beta_4 \cdot \text{Gender} + \epsilon \tag{10}$$

where ϵ is zero mean Gaussian noise. The age and gender effects are determined by testing the significance of β_3 and β_4 terms.

On the amygdala volume, we did not find the significant effect of age (Left: p= 0.31; Right: p= 0.15; Total: p= 0.20; Figure 4, upper row) nor gender (Left: p= 0.20; Right: p= 0.35; Total: p= 0.25; Figure 4, lower row). Either on the hippocampus volume, we did not find a significant effect of age (Left: p= 0.92; Right: p= 0.90; Total: p= 0.90; Figure 5, upper row). However, we found a significant effect of gender (Left: p= 0.05; Right: p= 0.04; Total: p= 0.03; Figure 5, lower row).

3.2 Localized surface shape analysis

The lengths of displacement vector fields along the template surfaces were estimated and smoothed as previously described in section 2. The same GLMs and variables as in section 3.1 were used once again, except that the measures are the lengths of displacement vector field. Using SurfStat MATLAB toolbox (http://www.math.mcgill.ca/keith/surfstat/), random field corrected p-values were thresholded at 0.01.

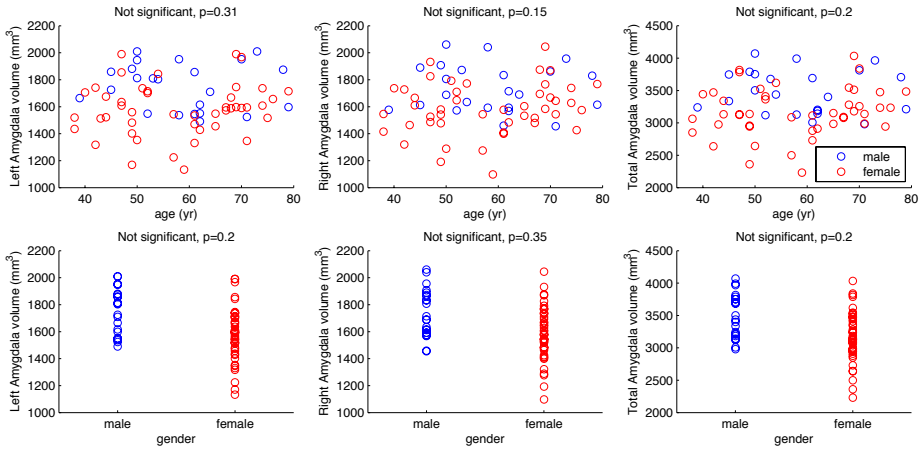

Fig. 4. Scatterplots of left, right and combined amygdala volumes against age (upper row) and gender (lower row).

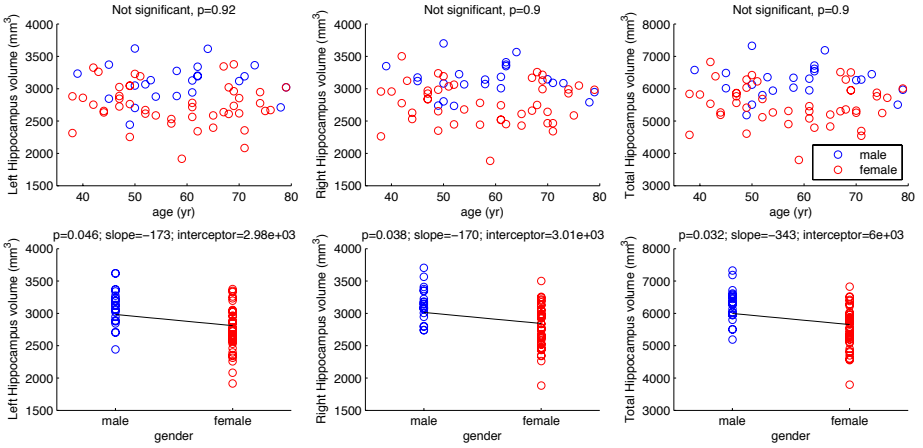

Fig. 5. Scatterplots of the volume of left, right and total hippocampus against age (upper row) and gender (lower row).

We found significant effects of age on the posterior part of hippocampi (Left: max(F)=39.43, $p < 10^{-5}$; Right: max(F)=23.11, p=0.002; Fig 6) but no age effects on the amygdalae. Also we found a small region that differed between gender groups on the inferior part of the right amygdala (max(F)=24.66, p <0.001; Fig 6). However we did not find any significant gender effects on the other structures.

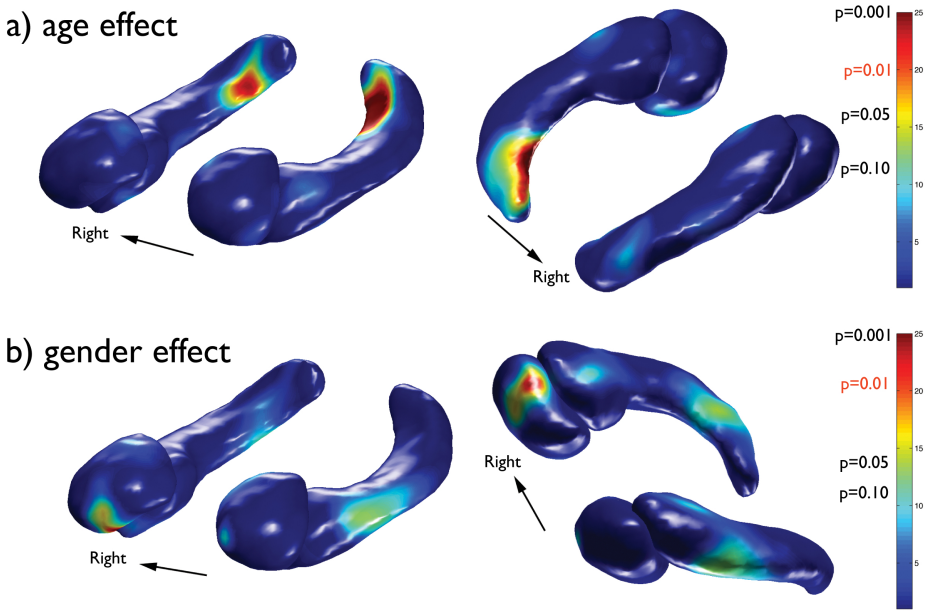

Fig. 6. F-statistic maps on the template surfaces for the age effect (a) and the gender effect (b). Corresponding corrected p-values are indicated. Note that we accept $p < 0.01$ as significant in this paper.

4 Discussion

4.1 Anatomical findings

We have presented a shape analysis framework for investigating relevant factors that affect the shape of subcortical structures, comparing with the traditional volumetric analysis.

Age effect The traditional volumetric analysis could not find any significant effects of age on the hippocampi and amygdalae. However, we found a significant effects of age using the proposed shape analysis framework. Particularly, on the caudal regions of the left and right hippocampi, we found a highly localized signals. It is consistent with other shape modeling studies [29,18].

Gender effect In volumetric analysis, we find a significant effect of gender in terms of the hippocampus volume, although we could not verify the finding in shape modeling analysis. However, interestingly, we found a gender effect on the right amygdala, which we did not found using volumetric analysis. Although further examination is necessary for this finding, but it demonstrates the advantage of the proposed framework.

4.2 Methodological considerations

References

1. LeDoux, J.: The amygdala. Current Biology **17**(20) (2007) R868 – R874
2. Alvarez, P., Squire, L.R.: Memory consolidation and the medial temporal lobe: a simple network model. Proceedings of the National Academy of Sciences **91**(15) (1994) 7041–7045
3. Miller, A., Alston, R., Corsellis, J.: Variation with age in the volumes of grey and white matter in the cerebral hemispheres of man: measurements with an image analyser. Neuropathology and applied neurobiology **6**(2) (1980) 119–132
4. Good, C., Johnsrude, I., Ashburner, J., Henson, R., Friston, K., Frackowiak, R.: A voxel-based morphometric study of ageing in 465 normal adult human brains. Neuroimage **14**(1) (2001) 21–36
5. Walhovd, K., Westlye, L., Amlien, I., Espeseth, T., Reinvang, I., Raz, N., Agartz, I., Salat, D., Greve, D., Fischl, B., et al.: Consistent neuroanatomical age-related volume differences across multiple samples. Neurobiology of Aging (2009)
6. Bigler, E., Blatter, D., Anderson, C., Johnson, S., Gale, S., Hopkins, R., Burnett, B.: Hippocampal volume in normal aging and traumatic brain injury. American Journal of Neuroradiology **18**(1) (1997) 11
7. Du, A., Schuff, N., Chao, L., Kornak, J., Jagust, W., Kramer, J., Reed, B., Miller, B., Norman, D., Chui, H., et al.: Age effects on atrophy rates of entorhinal cortex and hippocampus. Neurobiology of aging **27**(5) (2006) 733–740
8. Walhovd, K., Fjell, A., Reinvang, I., Lundervold, A., Dale, A., Eilertsen, D., Quinn, B., Salat, D., Makris, N., Fischl, B.: Effects of age on volumes of cortex, white matter and subcortical structures. Neurobiology of Aging **26**(9) (2005) 1261–1270
9. Sullivan, E., Marsh, L., Mathalon, D., Lim, K., Pfefferbaum, A.: Age-related decline in mri volumes of temporal lobe gray matter but not hippocampus. Neurobiology of Aging **16**(4) (1995) 591–606
10. Sullivan, E., Marsh, L., Pfefferbaum, A.: Preservation of hippocampal volume throughout adulthood in healthy men and women. Neurobiology of aging **26**(7) (2005) 1093
11. Good, C., Johnsrude, I., Ashburner, J., Henson, R., Friston, K., Frackowiak, R.: Cerebral asymmetry and the effects of sex and handedness on brain structure: a voxel-based morphometric analysis of 465 normal adult human brains. Neuroimage **14**(3) (2001) 685–700
12. Gur, R.C., Gunning-Dixon, F., Bilker, W.B., Gur, R.E.: Sex differences in temporolimbic and frontal brain volumes of healthy adults. Cerebral Cortex **12**(9) (2002) 998–1003
13. Chung, M., Worsley, K., Paus, T., Cherif, D., Collins, C., Giedd, J., Rapoport, J., , Evans, A.: A unified statistical approach to deformation-based morphometry. NeuroImage **14** (2001) 595–606

14. Ashburner, J., Friston, K.: Voxel-based morphometry–the methods. Neuroimage **11**(6) (2000) 805–821
15. Ashburner, J., Friston, K.: Why voxel-based morphometry should be used. Neuroimage **14**(6) (2001) 1238–1243
16. Chung, C.M., Worsley, K., Robbins, S., Paus, T., Taylor, J., Giedd, J., Rapoport, J., Evans, A.: Deformation-based surface morphometry applied to gray matter deformation. NeuroImage **18** (2003) 198–213
17. Styner, M., Lieberman, J., Pantazis, D., Gerig, G.: Boundary and medial shape analysis of the hippocampus in schizophrenia. Medical Image Analysis **8**(3) (2004) 197–203
18. Qiu, A., Miller, M.: Multi-structure network shape analysis via normal surface momentum maps. NeuroImage **42**(4) (2008) 1430–1438
19. Chung, M.K., Worsley, K.J., Nacewicz, B.M., Dalton, K.M., Davidson, R.J.: General multivariate linear modeling of surface shapes using surfstat. NeuroImage **53**(2) (2010) 491 – 505
20. Smith, S.: Fast robust automated brain extraction. Human Brain Mapping **17**(3) (2002) 143–155
21. Avants, B., Epstein, C., Grossman, M., Gee, J.: Symmetric diffeomorphic image registration with cross-correlation: Evaluating automated labeling of elderly and neurodegenerative brain. Medical Image Analysis **12**(1) (2008) 26–41
22. Lorensen, W., Cline, H.: Marching cubes: A high resolution 3d surface construction algorithm. ACM Siggraph Computer Graphics **21**(4) (1987) 163–169
23. Qiu, A., Bitouk, D., Miller, M.: Smooth functional and structural maps on the neocortex via orthonormal bases of the laplace-beltrami operator. Medical Imaging, IEEE Transactions on **25**(10) (2006) 1296–1306
24. Seo, S., Chung, M., Vorperian, H.: Heat kernel smoothing using laplace-beltrami eigenfunctions. Medical Image Computing and Computer-Assisted Intervention–MICCAI 2010 (2010) 505–512
25. Lévy, B.: Laplace-beltrami eigenfunctions towards an algorithm that understands geometry. In: Shape Modeling and Applications, 2006. SMI 2006. IEEE International Conference on, IEEE (2006) 13–13
26. Chung, M., Robbins, S., Dalton, K., Davidson, R., Alexander, A., Evans, A.: Cortical thickness analysis in autism with heat kernel smoothing. NeuroImage **25**(4) (2005) 1256–1265
27. Tasdizen, T., Whitaker, R., Burchard, P., Osher, S.: Geometric surface smoothing via anisotropic diffusion of normals. Visualization Conference, IEEE **0** (2002) null
28. Chung, M., Dalton, K., Shen, L., Evans, A., Davidson, R.: Weighted fourier series representation and its application to quantifying the amount of gray matter. Medical Imaging, IEEE Transactions on **26**(4) (2007) 566–581
29. Xu, Y., Valentino, D., Scher, A., Dinov, I., White, L., Thompson, P., Launer, L., Toga, A.: Age effects on hippocampal structural changes in old men: the haas. Neuroimage **40**(3) (2008) 1003–1015